CHARMM-GUI Supports Hydrogen Mass Repartitioning and Different Protonation States of Phosphates in LPS

Ya Gao[1†], Jumin Lee[2†], Iain Peter Shand Smith[3†], Hwayoung Lee[2†], Seonghoon Kim[2,4], Yifei Qi[5], Jeffery B. Klauda[6], Göran Widmalm[7], Syma Khalid[3], and Wonpil Im[2*]

[†]These authors contributed equally to this work.

[1]School of Mathematics, Physics and Statistics, Shanghai University of Engineering Science, Shanghai 201620, China

[2]Department of Biological Sciences, Department of Chemistry, Department of Bioengineering, and Department of Computer Science and Engineering, Lehigh University, Bethlehem, PA 18015, USA

[3]School of Chemistry, University of Southampton, Southampton, S017 1BJ, UK

[4]School of Computational Sciences, Korea Institute for Advanced Study, Seoul 02455, Republic of Korea

[5]Shanghai Engineering Research Center of Molecular Therapeutics and New Drug Development, School of Chemistry and Molecular Engineering, East China Normal University, Shanghai, 200062, China

[6]Department of Chemical and Biomolecular Engineering and the Biophysics Program, University of Maryland College Park, Maryland 20742, USA

[7]Department of Organic Chemistry, Arrhenius Laboratory, Stockholm University, SE-10691 Stockholm, Sweden

*Correspondence: wonpil@lehigh.edu

ABSTRACT

Hydrogen mass repartitioning (HMR) that permits time steps of all-atom molecular dynamics simulation up to 4 fs by increasing the mass of hydrogen atoms has been used in protein and phospholipid bilayers simulations to improve conformational sampling. Molecular simulation input generation via CHARMM-GUI now supports HMR for diverse simulation programs. In addition, considering ambiguous pH at the bacterial outer membrane surface, different protonation states, either -2*e* or -1*e*, of phosphate groups in lipopolysaccharides (LPS) are also supported in CHARMM-GUI *LPS Modeler*. To examine the robustness of HMR and the influence of protonation states of phosphate groups on LPS bilayer properties, eight different LPS-type all-atom systems with two phosphate protonation states are modeled and simulated utilizing both OpenMM 2-fs (standard) and 4-fs (HMR) schemes. Consistence in the conformational space sampled by standard and HMR simulations shows the reliability of HMR even in LPS, one of the most complex biomolecules. For systems with different protonation states, similar conformations are sampled with a PO_4^{1-} or PO_4^{2-} group, but different phosphate protonation states make slight impacts on lipid packing and conformational properties of LPS acyl chains. Systems with PO_4^{1-} have slightly smaller area per lipid and thus slightly more ordered lipid A acyl chains compared to those with PO_4^{2-}, due to more electrostatic repulsion between PO_4^{2-} even with neutralizing Ca^{2+} ions. HMR and different protonation states of phosphates of LPS available in CHARMM-GUI are expected to be useful for further investigations of biological systems of diverse origin.

INTRODUCTION

Conventional all-atom molecular dynamics (MD) simulations suffer from slow and incomplete coverage of phase space, which can limit their applicability to slowly evolving systems. Thus, there is a great need to identify and implement methods to improve conformational sampling.[1-4] A major contributing factor to the slow coverage of phase space is the small integration time-steps (1 or 2 fs) that are required to conserve the total energy.[5] Hydrogen mass repartitioning (HMR) is a simulation technique that enables all-atom MD to employ a 4-fs time-step by distributing a heavy atom mass to hydrogen atom(s) attached to the heavy atom. It was originally proposed by Feenstra et al. in 1999[5] and was shown to be practically useful for protein simulations by Hopkins et al. in 2015.[6] Among different HMR schemes, the most popular one is to increase each hydrogen atom mass by a factor of 3 and subtract the total increased mass from the heavy atom bearing hydrogen atom(s). HMR has become popular in the MD simulation community with its recent application to phospholipid bilayers.[7-9] CHARMM-GUI (http://www.charmm-gui.org)[10-11] now supports this HMR scheme for NAMD[12], GROMACS[13], AMBER[14], GENESIS[15], LAMMPS[16], Desmond[17], and OpenMM[18]. In this work, we have tested the HMR scheme by performing MD simulations of various lipopolysaccharide (LPS) bilayer systems using OpenMM.

LPS molecules, which are found in the outer leaflet of the outer membranes (OM) of Gram-negative bacteria, are composed of lipid A, core oligosaccharide, and O-antigen polysaccharide, representing one of the most complex biological molecules.[19-20] In LPS, phosphate groups are often attached to the glucosamine dimer of lipid A and L-glycero-D-manno-heptose (Hep) of a core oligosaccharide. At 25 °C, two pK_a values of glucose-1-phosphate and glucose-4-phosphate are 1.10/6.13 and 0.84/5.67, respectively.[21-22] Under physiological conditions, however, the protonation states, either -2*e* or -1*e*, of phosphate groups in LPS are difficult to be determined unambiguously due to unknown pH at the bacterial OM surface. Therefore, *LPS Modeler*[23-24] and *Membrane Builder*[25-27] in CHARMM-GUI now supports different protonation states of LPS phosphate groups. In this work, the influences of different protonation states on LPS bilayer properties have been extensively tested by performing MD simulations of various LPS bilayer systems. Note that this work was partially motivated by a recent simulation study by Amy et al. that explored the influence of the protonation states of lipid A glucosamine phosphate groups on the properties of bilayers composed of *Salmonella enterica* lipid A and Rc core (two Kdo (2-keto-3-deoxyoctulosonate), three Hep, and one Glc (D-glucose)).[28] Among many recent progresses in MD simulations of various LPS systems[29-31], their study is the first work (to the best of our knowledge) to investigate the different phosphate protonation states and LPS-ion interactions.

In this work, as shown in **Table 1**, eight different LPS-type systems were modeled and simulated: three from *Pseudomonas aeruginosa* (*P. aeruginosa* or Pa), two from *Escherichia coli* (*E. coli* or Ec), and three from *Burkholderia cepacia* (*B. cepacia* or Bc). These LPS types differ by lipid A, core, and O-antigen regions, such that extensive simulations of these complex LPS bilayers are valuable in order to examine the usage of HMR, as well as the influences of phosphate protonation states on LPS bilayer properties.

Table 1. LPS system information in this study.[†]

System name	LPS type
Pa-Kdo	*P. aeruginosa* lipid A + 2 Kdo sugars
Pa-G2	*P. aeruginosa* lipid A + core 2
Pa-O10	*P. aeruginosa* lipid A + core 2 + 2 repeating units of O10 O-antigen
Ec-Kdo	*E. coli* lipid A + 2 Kdo sugars
Ec-K12	*E. coli* lipid A + K12 core

Bc-T1	*B. cepacia* lipid A (Type 1) + core A
Bc-T2	*B. cepacia* lipid A (Type 2) + core A
Bc-T3	*B. cepacia* lipid A (Type 3) + core A

[†]Unless specified explicitly, lipid A is type 1 defined in CHARMM-GUI *LPS Modeler*. LPS structures are shown in **Figure S1**.

METHODS

System details

To investigate the effects of LPS phosphate protonation states on the outer leaflet of bacterial OMs, symmetric bilayers with different LPS types (**Table 1**) were modeled and simulated. For *P. aeruginosa* systems, three different systems were built: Pa-Kdo with *P. aeruginosa* lipid A and two Kdo residues, Pa-G2 with lipid A and G2 core oligosaccharides, and Pa-O10 with lipid A, G2 core, and two repeating units of O-10 O-antigen (hereinafter, O10-antigen). All symmetric bilayers with 49 LPS molecules in each leaflet were constructed using *Membrane Builder* in CHARMM-GUI. Ca^{2+} ions were added to the LPS lipid A and core regions to neutralize each system and 150 mM KCl was added to the bulk region to mimic the bulk ionic solution. An initial area per lipid (APL) of 180 $Å^2$ was used in the modeling of Pa-Kdo and Pa-G2 systems, while both 180 $Å^2$ and 200 $Å^2$ APL were used for the Pa-O10 system (Pa-$O10^{180}$ and Pa-$O10^{200}$) to check the simulation convergence depending on the initial membrane area (**Figure 1**). For each Pa system, both protonation states, either -2*e* or -1*e*, of phosphate groups in the glucosamine dimer of lipid A (**Figure S2**) were considered.

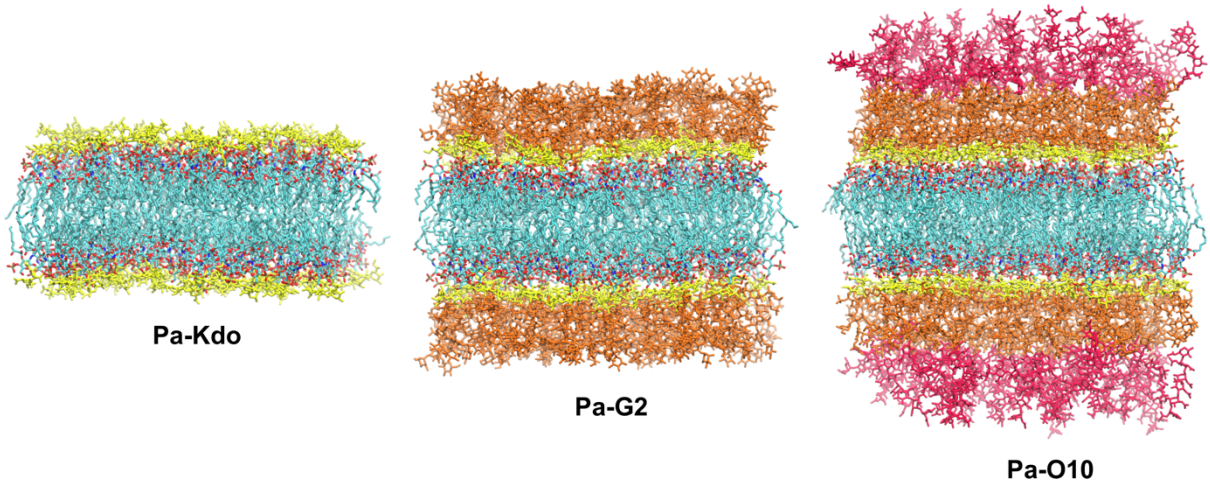

Figure 1. Molecular graphics snapshots of systems Pa-Kdo, Pa-G2, and Pa-O10. Lipid A in each LPS is colored by atom: cyan for carbon, red for oxygen, blue for nitrogen, and tan for phosphorus. Kdo residues are colored yellow. The G2 core is colored yellow and orange, and two O10 polysaccharide repeating units are colored red.

E. coli and *B. cepacia* systems were prepared with the same procedure used for *P. aeruginosa* systems. A total of 49 LPS molecules were added in each leaflet to model symmetric systems. For the *E. coli* systems, two different systems were built: Ec-Kdo with *E. coli* lipid A and two Kdo residues and Ec-K12 with lipid A and K-12 core oligosaccharides. Like in the Pa system, two

protonation states (-2*e* or -1*e*) of phosphate groups in the glucosamine dimer of lipid A were considered. For Ec-K12 systems, in addition to lipid A, different phosphate protonation states were also considered for Hep residues in the K12 core (Ec-K12^a and Ec-K12^b for Hep with -2*e* or -1*e* phosphate group, respectively). For *B. cepacia* systems, the same core oligosaccharide sequence was used with a variation in lipid A structures (**Figure S3**). Type 1 lipid A includes penta-acylated tails and two phosphate groups on each end of the glucosamine dimer. Both phosphate groups were assigned to two different protonation states, -2*e* or -1*e*, in different simulations. Type 2 lipid A has an additional 4-amino-4-deoxy-L-arabinose (L-Ara4N) connected to the first phosphate group. The second phosphate group was assigned to -2*e* or -1*e*. Type 3 lipid A has an additional L-Ara4N at both phosphate groups, making the net charge neutral. An initial APL of 200 Å was used for both *E. coli* and *B. cepacia* systems.

Simulation details

During simulations, together with a TIP3P water model,[32-33] the CHARMM36 force field for LPS[24, 34], lipids[35], and carbohydrates[36-40] was used to describe the system energetics. For each system, following the CHARMM-GUI standard membrane equilibration protocol, equilibrations were first conducted in NVT (constant particle number, volume, and temperature) ensemble with gradually decreasing restraints applied to the lipids and water molecules to ensure the gradual equilibration of the assembled system. After equilibration, 2-μs (Pa systems), 1.5-μs (Ec systems), or 2.5-μs (Bc systems) NPT (constant particle number, pressure, and temperature) production simulation with a time-step of 2 fs was conducted for each system. During simulations, all bonds containing hydrogen atoms were fixed using SHAKE.[41] The van der Waals interactions were smoothly switched off over 10–12 Å by a force-switching function[42] and the long-range electrostatic interactions were calculated using the particle-mesh Ewald method.[43] For OpenMM simulations, Langevin dynamics was used for the temperature coupling with a collision frequency of 1 ps^{-1}. A semi-isotropic Monte Carlo barostat method with a pressure coupling frequency of 100 steps was used to maintain the pressure.[44-45] Unless specified explicitly, for all simulations, the temperature was maintained at 310.15 K and the pressure was set to 1 bar. For HMR simulations, all simulation details were the same as the standard ones except for 4-fs time-step used in production runs. Three independent replicas with different random seed numbers were simulated to improve sampling and to check the simulation convergence.

RESULTS AND DISCUSSION

The simulation results are presented in the following order: (1) results of Pa, Ec, and Bc systems with different phosphate protonation states using OpenMM 2-fs time-step; (2) results of Pa systems using OpenMM 4-fs time-step with HMR.

Influences of different phosphate protonation states on conformational preference

For each Pa system, comparisons of pairwise root-mean-square deviation (RMSD of the entire LPS including the acyl chain after superposition) calculated between 1.0 – 1.5 μs and 1.5 – 2.0 μs are shown in **Figure S4**. The RMSD distributions are almost identical between the two time periods, indicating simulations reach convergence and similar conformational ensembles are sampled during last 1-μs simulations with either PO_4^{1-} or PO_4^{2-} groups. As expected, the Pa-O10 systems are more dynamic and flexible with broader RMSD distributions compared to Pa-G2 and Pa-Kdo systems due to its large size. In the following, unless specified explicitly, the last 500-ns trajectories are used for analyses.

To investigate the influence of phosphate protonation states on the conformational variations, pairwise RMSD distributions with PO_4^{1-} and PO_4^{2-} groups are shown in **Figure 2A**. The well overlapped distributions for each system indicate that similar conformational ensembles are sampled and no significant structural variations are observed between the two protonation states. The averaged Z-lengths between phosphate groups of lipid A and the first residue of each O10-antigen repeating unit are shown in **Figure 2C**; there are two O10 repeating units in Pa-O10 systems. In both protonation states, conformations with similar Z-lengths (about 26 ± 2 Å and 34 ± 4 Å, respectively) are sampled during simulations, which is consistent with the result of pairwise RMSD distributions. Thus, although different protonation states are used for lipid A, each Pa system adopts similar conformation with PO_4^{1-} or PO_4^{2-}. For Ec and Bc systems, similar pairwise RMSD distributions are also observed between two protonation states (**Figure S5**), consistent with the conclusion for Pa systems that similar conformations are sampled with PO_4^{1-} or PO_4^{2-} groups.

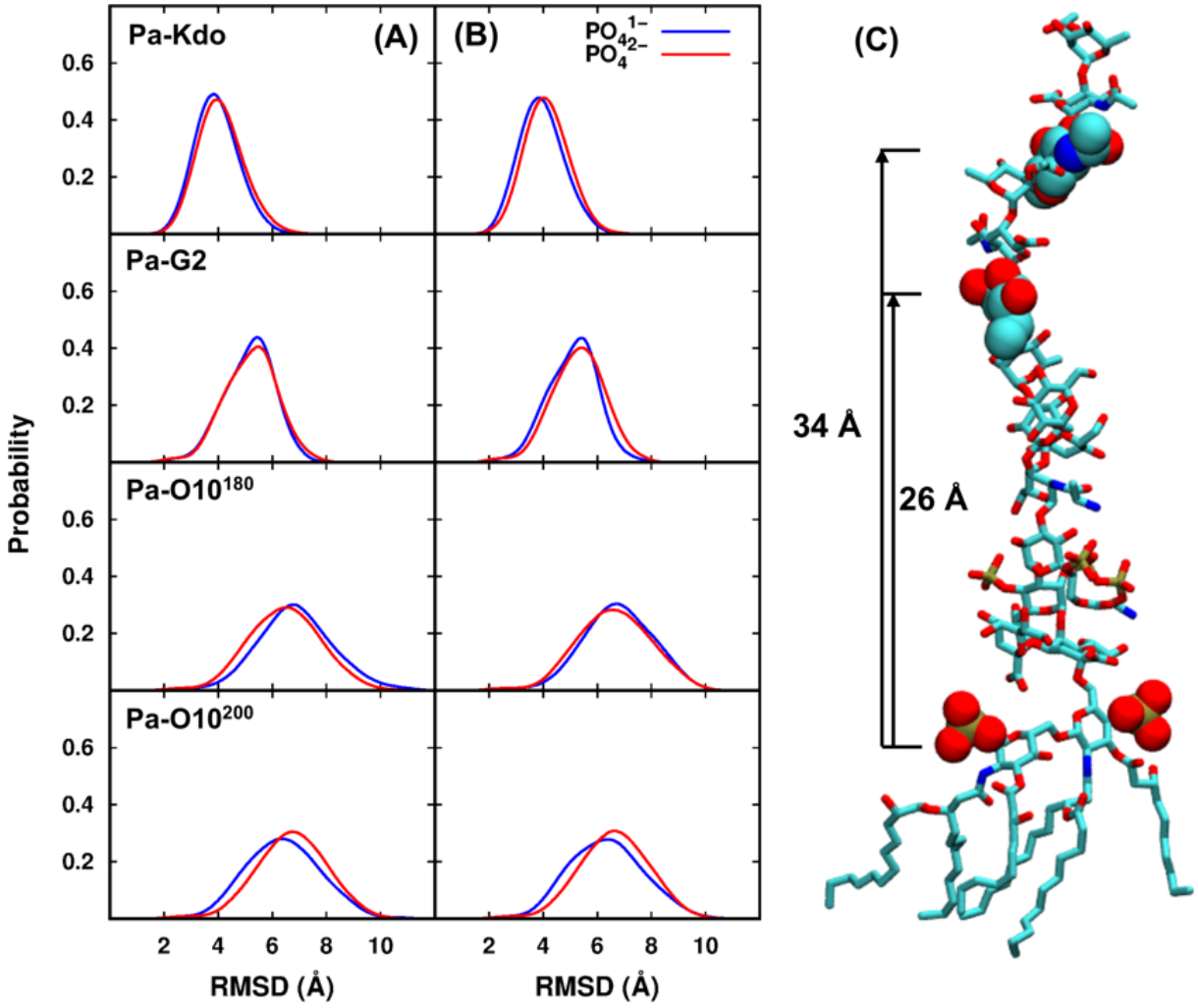

Figure 2. Comparisons of pairwise RMSD distributions between two phosphate protonation states in (A) standard and (B) HMR simulations for each Pa system. Pa-$O10^{180}$ and Pa-$O10^{200}$ denote the systems with the initial areas per lipid of 180 $Å^2$ and 200 $Å^2$, respectively. (C) Averaged Z-lengths between the centers of mass of phosphate groups of lipid A and the first residue of each O10-antigen repeating unit. The structure is a snapshot from Pa-O10 with PO_4^{1-}.

Different protonation states of lipid A phosphate groups could also alter the distributions of divalent cations that maintain the stability and integrity of LPS membrane systems. **Figure S6A** and **Figure S7** show the density distributions of Ca^{2+} ions along the Z axis (i.e., the membrane normal with the bilayer center at Z = 0) for Pa, Ec, and Bc systems. Ca^{2+} ions are dominantly occupied in the lipid headgroup and core regions. For Pa-O10 systems, some Ca^{2+} ions moved slightly toward the O10-antigen region indicated by the small peak at Z = 46 Å. As expected, when phosphate group charges are -2*e*, more Ca^{2+} ions are bound to the lipid A phosphate regions (around Z = 17 Å) for each Pa system simply because there are more neutralizing Ca^{2+} ions. Comparison between Ec-K12[a] and Ec-K12[b] systems also indicates more Ca^{2+} ions bound in the core region due to the -2*e* phosphate charge for HEP residues in Ec-K12[a].

Influences of different phosphate protonation states on bilayer properties

Although similar conformations are sampled with PO_4^{1-} and PO_4^{2-} groups for each system, different phosphate protonation states could make impacts on lipid packing and conformational properties of LPS acyl chains. **Figure S8** shows the time series of averaged area per lipid (APL) every 100 ns and its corresponding standard errors for each Pa system in both protonation states. Both averaged APL and its standard errors (**Table S1**) generally reach a plateau after about 1-μs simulation. It is noticeable that systems with PO_4^{1-} have slightly smaller APL compared to those with PO_4^{2-}, indicating the lipid A acyl chains are slightly more ordered and straight with PO_4^{1-}. In addition, for systems Pa-$O10^{180}$ and Pa-$O10^{200}$ started with two different initial APL values, there still exists slight differences for the averaged APL (even after 2-μs simulation), which results from the slow lateral relaxation of LPS. The hydrophobic thicknesses calculated using carbons in the purple circles in **Figure S2** are shown in **Figure 3A** and **Table S1**. Expected from the APL results, the hydrophobic thickness of each Pa system with PO_4^{2-} is slightly thinner than the corresponding Pa system with PO_4^{1-}.

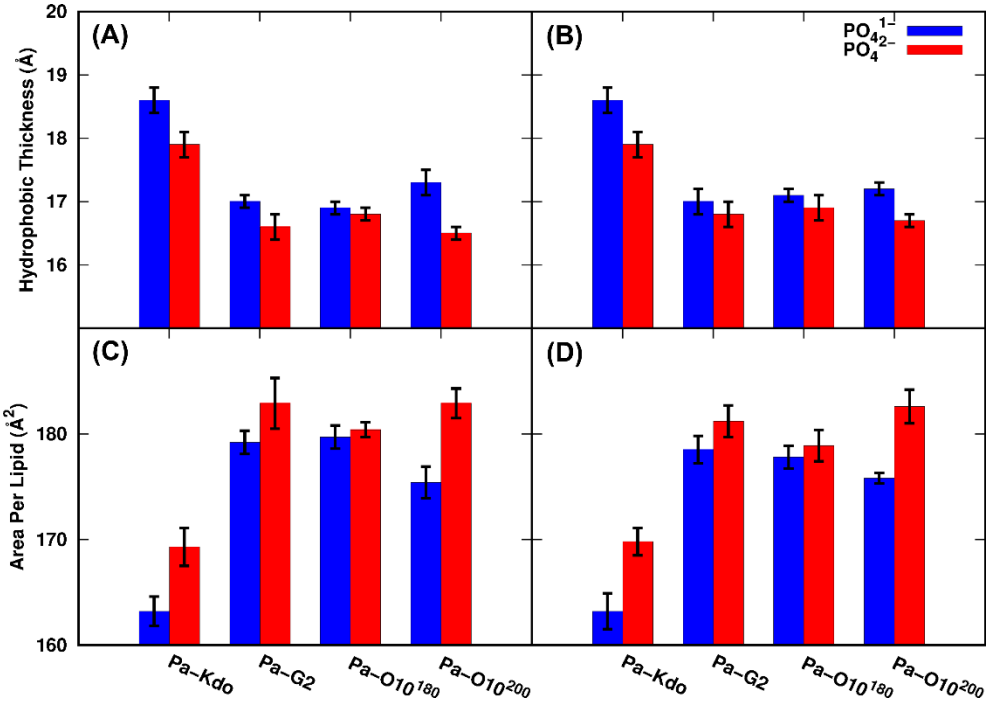

Figure 3. Averaged hydrophobic thickness and area per lipid for each Pa system with two phosphate protonation states: (A and C) standard and (B and D) HMR simulations.

For Ec systems, averaged APL along with simulation time generally reach convergence after 1-μs as shown in **Figure S9**. However, there still exists significant differences for simulations of Bc systems among the three replicas, which clearly manifests the slow lateral relaxation of these LPS types. In this work, for Bc systems, temperature was increased to 400 K at 500 ns and then cooled down to 310 K at 1.5 μs to obtain better convergence as shown in **Figure S9**. The last 500-ns trajectories at 310 K were used for analyzes. Averaged APL and its standard error are shown in **Table S2.** Except for Bc-T2 systems, averaged APL with PO_4^{1-} groups are all smaller than those with PO_4^{2-}, and hydrophobic thickness is correspondingly larger, which is consistent with the Pa results. For Bc-T2 systems, there is only one phosphate group having -2*e* or -1*e* (**Figure S3**), and the APL difference is within the errors. For Ec-K12 systems, it is also found that the APL becomes larger when the phosphate group of Hep is -2*e*, regardless of the lipid A protonation state. Results from analysis of APL and hydrophobic thickness indicate that the protonation state of phosphate groups in lipid A could affect the lipid packing and conformations of acyl chains of lipid A.

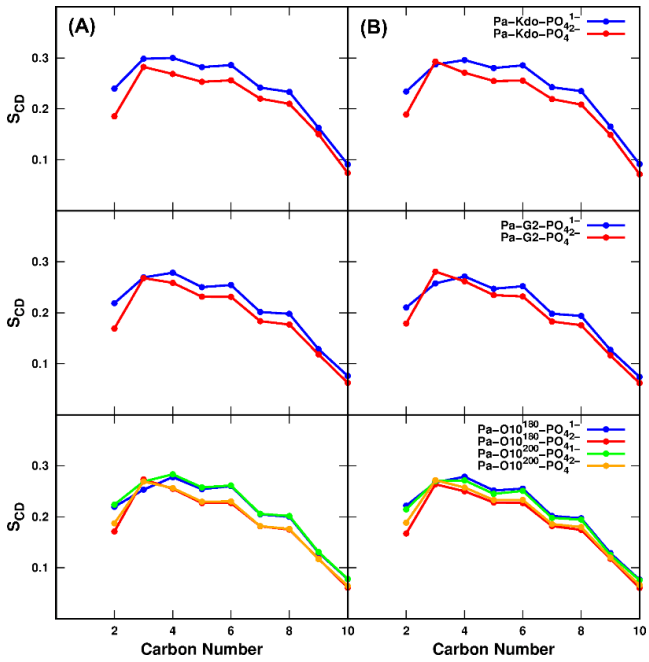

Figure 4. Calculated chain order parameters for acyl chain 3 of lipid A for each Pa system with two phosphate protonation states: (A) standard and (B) HMR simulations.

The order parameters (S_{CD}) of lipid acyl chains are also used to provide information regarding the overall order of the membrane. $S_{CD} = |< 3 \times \cos^2(\theta_{CH}) - 1 >/2|$, where θ_{CH} is the angle between a C-H bond vector and the Z axis, and the bracket represents the time and ensemble average. **Figure 4A** shows the calculated S_{CD} of lipid A acyl chain 3 (in **Figure S2**) in each Pa system. Overall, the acyl chain is more ordered with PO_4^{1-} compared to that with PO_4^{2-}, indicated by larger S_{CD} values. The lipid A analysis again agrees well with the hydrophobic thickness and APL results, indicating that LPS bilayers with PO_4^{2-} in lipid A are slightly more dynamic and flexible. S_{CD} of acyl

chain 2 for Ec and Bc systems are also calculated and plotted in **Figure S10**. The more ordered acyl chains with PO_4^{1-} groups are detected for Ec and Bc systems, which is consistent with the conclusion from the Pa systems.

The protonation state of lipid A phosphate groups also affects the electrostatic interactions among LPS as well as between LPS and divalent cations. **Figure 5A** shows the sum of the per-LPS average number of inter-lipid A hydrogen bonds and the per-LPS average salt bridges between Ca^{2+} and phosphate groups for Pa systems (see **Figure S11** for Ec and Bc systems). For Pa systems with PO_4^{1-}, more inter-lipid A hydrogen bonds are detected than those with PO_4^{2-} due to more hydrogen bond donors in PO_4^{1-} (**Figure S12A**). However, the overall stabilization of the leaflet integrity is maintained by the electrostatic interactions formed by salt bridges between Ca^{2+} ions and phosphate groups of lipid A, indicated by much larger number of salt bridges than that of inter-lipid A hydrogen bonds (**Figure S12C**). While there are more salt bridges for the PO_4^{2-} cases due to more neutralizing Ca^{2+} ions, stronger electrostatic repulsion between PO_4^{2-} groups appears to make the APL of LPS with PO_4^{2-} larger than that with PO_4^{1-}.

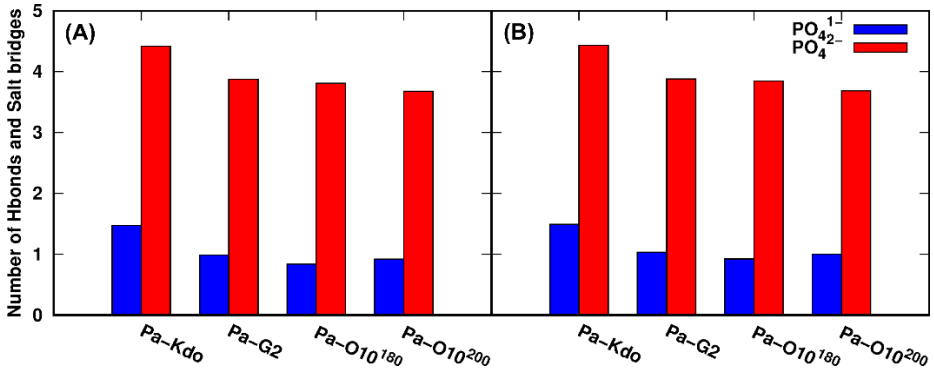

Figure 5. Sum of the per-LPS average number of inter-lipid A hydrogen bonds and the per-LPS average salt bridges between Ca^{2+} and phosphate groups for two phosphate protonation states: (A) standard and (B) HMR simulations. A hydrogen bond is counted when the distance between the donor and acceptor is less than 3 Å and the angle is larger than 120º. A salt bridge is counted when the distance between Ca^{2+} and any atom on phosphate groups of lipid A is less than 4 Å.

Axial relaxation time constants, which are related to both lipid structure and the membrane environment, are measured by the second-rank reorientational correlation function, $C_2(t)$, for specific atoms.

$$C_2(t) =< P_2[\hat{\boldsymbol{\mu}}(0) \cdot \hat{\boldsymbol{\mu}}(t)] >$$

where P_2 is the second Legendre polynomial and $\hat{\boldsymbol{\mu}}$ is a heavy atom vector. In this work, the vectors between the last carbons of each acyl chain were selected to estimate the slow relaxation time: C1.12 (12^{th} carbon from the carbonyl carbon in chain 1 in **Figure S2**) – C2.9, C3.10–C4.10, C4.12– C5.9, and C1.10–C6.10. Three exponential fits were used to determine time constants for each cross-acyl chain:

$$C_2(t) = a_0 + \sum_{i=1}^{3} a_i \, e^{-t/\tau_i}$$

The time constants represent the fast and slow relaxation times associated with the lipid's fast isomerization and slow wobbling motions, respectively.[46-48] As shown in **Table 2**, for LPS

membrane systems, the relaxation time is much longer than bilayers comprised of dipalmitoylphosphatidylcholine (DPPC) lipids, for which the slow relaxation time is ~10 ns and the full rotational motion is an order of magnitude longer.[48] In this study, the slow relaxation time of adjacent chains is ~300 ns, and for the long-range vector (C1.10–C6.10), which represents the overall lipid rotational-like motion, the correlation is still very high during last 1-μs simulations (**Figure S13**), i.e., longer relaxation time than adjacent chain vectors.

Table 2. Average of three-exponential fitted relaxation time (in ns) of the cross-chain correlation function in standard and HMR simulations.

cross chain	OpenMM 2-fs			OpenMM HMR		
	τ_1	τ_2	τ_3	τ_1	τ_2	τ_3
C1.12-C2.9	0.36 ± 0.04	11.60 ± 2.23	328.7 ± 116.3	0.37 ± 0.02	11.23 ± 1.28	322.9 ± 50.36
C3.10-C4.10	0.38 ± 0.03	13.43 ± 1.01	294.0 ± 36.0	0.39 ± 0.03	14.15 ± 1.75	362.5 ± 36.78
C4.12-C5.9	0.38 ± 0.06	11.41 ± 2.38	335.2 ± 123.9	0.37 ± 0.06	10.56 ± 2.43	271.5 ± 64.92
C1.10-C6.10	0.59 ± 0.05	15.69 ± 1.54	398.0 ± 127.0	0.65 ± 0.07	18.07 ± 3.32	479.5 ± 194.2

Comparison between standard and HMR simulations for Pa systems

The HMR technique permits all-atom MD simulation time steps of up to 4 fs and thus improves simulation efficiency with reasonable stability. Since HMR is now available in CHARMM-GUI and can be used for various systems, the methodology was herein employed to perform simulations and examine its robustness by investigating the conformational properties for Pa systems. Pairwise RMSD distributions for two protonation states are shown in **Figure 2B**. Compared to standard 2-fs simulations, similar RMSD distributions with comparable probabilities are observed for each system. The averaged Z-lengths between phosphate groups in lipid A and the first residue of each O10-antigen repeating unit are also close to that in the standard simulations (~26 ± 2 Å and 34 ± 4 Å, respectively) for both protonation states, indicating that similar conformations are sampled under HMR and standard OpenMM simulations. In addition, consistent with standard simulations, the well overlapped pairwise-RMSD distributions with PO_4^{1-} or PO_4^{2-} indicate similar conformational space of LPS sampled under two protonation states. Density distributions of Ca^{2+} ions are shown in **Figure S6B**. Similar pairwise RMSD and Ca^{2+} ions distributions between HMR and standard simulations prove the usefulness of HMR.

Averaged APL and its corresponding standard errors under two protonation states from HMR simulations are summarized in **Table S1.** The APL under HMR is very close to those under standard simulations, and the difference between two simulations falls within its standard errors, indicating that a similar conformational ensemble is sampled under both HMR and standard simulations. For systems Pa-O10^{180} and Pa-O10^{200} there also exists slight differences for the averaged APL. Hydrophobic thickness, number of hydrogen bonds and salt bridges (**Figure 3B and Figure 5B**) are also consistent with those from the standard simulations. Relaxation times were also determined for HMR simulations to examine if the HMR method changes the lipid dynamics compared to standard simulations. **Table 2** indicates that HMR results are comparable with standard ones, indicating the reliability of HMR simulations.

CONCLUSIONS

The HMR and different protonation states of phosphates in LPS are now supported in CHARMM-GUI for various biomolecular MD simulations. In this work, eight different LPS-type systems were modeled and simulated utilizing standard OpenMM 2-fs and HMR 4-fs schemes to examine the

usage of HMR, as well as the influences of phosphate protonation states on LPS bilayer properties. Comparisons of pairwise RMSD distributions, area per lipid, hydrophobic thickness, chain order parameters, and number of inter-lipid hydrogen bonds between standard and HMR simulations reveal the robustness of HMR, supporting that HMR can be used for complex biomolecular simulations including LPS. For systems with two phosphate protonation states, similar conformations are sampled with either a PO_4^{1-} or PO_4^{2-} group, indicated by pairwise RMSD distributions. However, slight impacts on lipid packing and conformational properties of LPS acyl chains are also observed with Ca^{2+} neutralizing ions. Systems with PO_4^{1-} group(s) have slightly smaller area per lipid and thus slightly more ordered lipid A acyl chains compared to those with PO_4^{2-}. More hydrogen bonds between Lipid A molecules are detected in the PO_4^{1-} case than the PO_4^{2-} case due to more hydrogen bond donors in PO_4^{1-} groups. However, the stabilization of the leaflet integrity is dominated by the electrostatic interactions between Ca^{2+} ions and phosphate groups of lipid A, supported by the much larger number of salt bridges than of inter-lipid A hydrogen bonds. Axial relaxation time constants were determined by fitting the second-rank reorientational correlation functions of cross acyl chains; for LPS systems, the slow relaxation time (~300 ns) is much longer than bilayers comprised of phospholipids (~10 ns), indicating the slow lateral relaxation of LPS systems that is also manifested by slight APL differences even after 2-μs simulations of the systems with two different initial APL values. The availability of HMR and different protonation states of phosphates of LPS in CHARMM-GUI are expected to be useful for MD studies of different biomolecular systems.

ACKNOWLEDGEMENT

This work was supported in part by grants from the NSF MCB-1810695, NSF DBI-1660380, NIH GM138472, XSEDE MCB070009, Friedrich Wilhelm Bessel Research Award from the Humboldt foundation (to WI), the Swedish Research Council 2017-03703 (GW), KIAS individual grant (CG080501) (SK), the National Natural Science Foundation of China (62072296) (YG), NSF CHE-2003912 and MCB-1951425 (to JBK), and Engineering and Physical Sciences Research Council, EP/R029407/1 (to SK).

SUPPORTING INFORMATION

Figure S1: Schematic structures of Pa-O10, Ec-K12, and Bc-T1/T2/T3 LPS. Figure S2-S3: Chemical structures of *P. aeruginosa* lipid A and three types of *B. cepacia* lipid A. Figure S4: Comparisons of pairwise RMSD distributions (of the entire LPS) with two phosphate protonation states between 1.0 – 1.5 μs and 1.5 – 2.0 μs standard simulations for each Pa system. Figure S5: Comparisons of pairwise RMSD distributions (of the entire LPS) between two phosphate protonation states for each Ec and Bc systems. Figure S6-7: Comparisons of distributions of Ca^{2+} ions along the Z-axis (i.e., the membrane normal) between two phosphate protonation states for each Pa systems (in standard and HMR simulations) and for each Ec and Bc systems. Figure S8-9: Time series of averaged APL every 100 ns for each Pa, Ec, and Bc systems in both protonation states and its corresponding standard errors. Figure S10: Calculated chain order parameters for acyl chain 2 of lipid A for each Ec and Bc system with two phosphate protonation states. Figure S11: Sum of the per-LPS average number of inter-lipid A hydrogen bonds and the per-LPS average salt bridges between Ca^{2+} and phosphate groups for each Ec and Bc system with two phosphate protonation states. Figure S12: Per-LPS average number of inter-lipid A hydrogen bonds and salt bridges between Ca^{2+} and any atom on phosphate groups of lipid A for each Pa system (standard and HMR simulations). Figure S13: Correlation function $C_2(t)$ for the cross acyl chains in Pa-O10 system. Table S1: Averaged area per lipid and hydrophobic thickness with standard errors for each Pa system in standard and HMR simulations with two phosphate

protonation states. Table S2: Averaged area per lipid and hydrophobic thickness with standard errors for each Ec/Bc system with two phosphate protonation states.

References

1. Saiz, L.; Klein, M. L., Computer Simulation Studies of Model Biological Membranes. *Acc. Chem. Res.* **2002,** *35*, 482-489.
2. Marrink, S. J.; Risselada, H. J.; Yefimov, S.; Tieleman, D. P.; de Vries, A. H., The Martini Force Field: Coarse Grained Model for Biomolecular Simulations. *J. Phys. Chem. B* **2007,** *111*, 7812-7824.
3. Wang, Y.; Markwick, P. R. L.; de Oliveira, C. A. F.; McCammon, J. A., Enhanced Lipid Diffusion and Mixing in Accelerated Molecular Dynamics. *Biophys. J.* **2012,** *102*, 3199-3207.
4. Shearer, J.; Marzinek, J. K.; Bond, P. J.; Khalid, S., Molecular Dynamics Simulations of Bacterial Outer Membrane Lipid Extraction: Adequate Sampling? *J. Chem. Phys.* **2020,** *153*, 044122.
5. Feenstra, K. A.; Hess, B.; Berendsen, H. J. C., Improving Efficiency of Large Time-Scale Molecular Dynamics Simulations of Hydrogen-Rich Systems. *J. Comput. Chem.* **1999,** *20*, 786-798.
6. Hopkins, C. W.; Le Grand, S.; Walker, R. C.; Roitberg, A. E., Long-Time-Step Molecular Dynamics through Hydrogen Mass Repartitioning. *J. Chem. Theory Comput.* **2015,** *11*, 1864-1874.
7. Olesen, K.; Awasthi, N.; Bruhn, D. S.; Pezeshkian, W.; Khandelia, H., Faster Simulations with a 5 Fs Time Step for Lipids in the Charmm Force Field. *J. Chem. Theory Comput.* **2018,** *14*, 3342-3350.
8. Balusek, C.; Hwang, H.; Lau, C. H.; Lundquist, K.; Hazel, A.; Pavlova, A.; Lynch, D. L.; Reggio, P. H.; Wang, Y.; Gumbart, J. C., Accelerating Membrane Simulations with Hydrogen Mass Repartitioning. *J. Chem. Theory Comput.* **2019,** *15*, 4673-4686.
9. Lee, J.; Hitzenberger, M.; Rieger, M.; Kern, N. R.; Zacharias, M.; Im, W., Charmm-Gui Supports the Amber Force Fields. *J. Chem. Phys.* **2020,** *153*.
10. Jo, S.; Kim, T.; Iyer, V. G.; Im, W., Charmm-Gui: A Web-Based Graphical User Interface for Charmm. **2008,** *29*, 1859-1865.
11. Lee, J.; Cheng, X.; Swails, J. M.; Yeom, M. S.; Eastman, P. K.; Lemkul, J. A.; Wei, S.; Buckner, J.; Jeong, J. C.; Qi, Y. F.; Jo, S.; Pande, V. S.; Case, D. A.; Brooks, C. L.; MacKerell, A. D.; Klauda, J. B.; Im, W., Charmm-Gui Input Generator for Namd, Gromacs, Amber, Openmm, and Charmm/Openmm Simulations Using the Charmm36 Additive Force Field. *J. Chem. Theory Comput.* **2016,** *12*, 405-413.
12. Phillips, J. C.; Braun, R.; Wang, W.; Gumbart, J.; Tajkhorshid, E.; Villa, E.; Chipot, C.; Skeel, R. D.; Kale, L.; Schulten, K., Scalable Molecular Dynamics with Namd. *J. Comput. Chem.* **2005,** *26*, 1781-1802.
13. Abraham, M. J.; Murtola, T.; Schulz, R.; Páll, S.; Smith, J. C.; Hess, B.; Lindahl, E., Gromacs: High Performance Molecular Simulations through Multi-Level Parallelism from Laptops to Supercomputers. *SoftwareX* **2015,** *1-2*, 19-25.
14. Case, D. A.; Cheatham, T. E.; Darden, T.; Gohlke, H.; Luo, R.; Merz, K. M.; Onufriev, A.; Simmerling, C.; Wang, B.; Woods, R. J., The Amber Biomolecular Simulation Programs. *J. Comput. Chem.* **2005,** *26*, 1668-1688.
15. Jung, J.; Mori, T.; Kobayashi, C.; Matsunaga, Y.; Yoda, T.; Feig, M.; Sugita, Y., Genesis: A Hybrid-Parallel and Multi-Scale Molecular Dynamics Simulator with Enhanced Sampling Algorithms for Biomolecular and Cellular Simulations. *Wiley Interdiscip. Rev. Comput. Mol. Sci.* **2015,** *5*, 310-323.

16. Plimpton, S., Fast Parallel Algorithms for Short-Range Molecular-Dynamics. *J. Comput. Phys.* **1995,** *117*, 1-19.
17. Bowers, K. J.; Chow, D. E.; Xu, H.; Dror, R. O.; Eastwood, M. P.; Gregersen, B. A.; Klepeis, J. L.; Kolossvary, I.; Moraes, M. A.; Sacerdoti, F. D.; Salmon, J. K.; Shan, Y.; Shaw, D. E. In *Scalable Algorithms for Molecular Dynamics Simulations on Commodity Clusters*, SC '06: Proceedings of the 2006 ACM/IEEE Conference on Supercomputing, 11-17 Nov.; 2006; pp 43-43.
18. Eastman, P.; Swails, J.; Chodera, J. D.; McGibbon, R. T.; Zhao, Y. T.; Beauchamp, K. A.; Wang, L. P.; Simmonett, A. C.; Harrigan, M. P.; Stern, C. D.; Wiewiora, R. P.; Brooks, B. R.; Pande, V. S., Openmm 7: Rapid Development of High Performance Algorithms for Molecular Dynamics. *Plos Comput. Biol.* **2017,** *13*.
19. Simpson, B. W.; Trent, M. S., Pushing the Envelope: Lps Modifications and Their Consequences. *Nat. Rev. Microbiol.* **2019,** *17*, 403-416.
20. Stahle, J.; Widmalm, G., Lipopolysaccharides of Gram-Negative Bacteria: Biosynthesis and Structural Aspects. *Trends Glycosci. Glyc.* **2019,** *31*, E159-E171.
21. Cori, C. F.; Colowick, S. P.; Cori, G. T., The Isolation and Synthesis of Glucose-1-Phosphoric Acid. *J. Biol. Chem.* **1937,** *121*, 465-477.
22. Pontis, H. G., Preface. In *Methods for Analysis of Carbohydrate Metabolism in Photosynthetic Organisms*, Pontis, H. G., Ed. Academic Press: Boston, 2017.
23. Lee, J.; Patel, D. S.; Stahle, J.; Park, S. J.; Kern, N. R.; Kim, S.; Lee, J.; Cheng, X.; Valvano, M. A.; Holst, O.; Knirel, Y. A.; Qi, Y. F.; Jo, S.; Klauda, J. B.; Widmalm, G.; Im, W., Charmm-Gui Membrane Builder for Complex Biological Membrane Simulations with Glycolipids and Lipoglycans. *J. Chem. Theory Comput.* **2019,** *15*, 775-786.
24. Jo, S.; Wu, E. L.; Stuhlsatz, D.; Klauda, J. B.; MacKerell, A. D.; Widmalm, G.; Im, W., Lipopolysaccharide Membrane Building and Simulation. In *Glycoinformatics*, Lütteke, T.; Frank, M., Eds. Springer New York: New York, NY, 2015.
25. Jo, S.; Kim, T.; Im, W., Automated Builder and Database of Protein/Membrane Complexes for Molecular Dynamics Simulations. *Plos One* **2007,** *2*.
26. Jo, S.; Lim, J. B.; Klauda, J. B.; Im, W., Charmm-Gui Membrane Builder for Mixed Bilayers and Its Application to Yeast Membranes. *Biophys. J.* **2009,** *97*, 50-58.
27. Wu, E. L.; Cheng, X.; Jo, S.; Rui, H.; Song, K. C.; Davila-Contreras, E. M.; Qi, Y. F.; Lee, J. M.; Monje-Galvan, V.; Venable, R. M.; Klauda, J. B.; Im, W., Charmm-Gui Membrane Builder toward Realistic Biological Membrane Simulations. *J. Comput. Chem.* **2014,** *35*, 1997-2004.
28. Rice, A.; Rooney, M. T.; Greenwood, A. I.; Cotten, M. L.; Wereszczynski, J., Lipopolysaccharide Simulations Are Sensitive to Phosphate Charge and Ion Parameterization. *J. Chem. Theory Comput.* **2020,** *16*, 1806-1815.
29. Im, W.; Khalid, S., Molecular Simulations of Gram-Negative Bacterial Membranes Come of Age. In *Annual Review of Physical Chemistry, Vol 71*, Johnson, M. A.; Martinez, T. J., Eds. 2020; Vol. 71, pp 171-188.
30. Messias, A.; Santos, D. E. S.; Pontes, F. J. S.; Lima, F. S.; Soares, T. A., Out of Sight, out of Mind: The Effect of the Equilibration Protocol on the Structural Ensembles of Charged Glycolipid Bilayers. *Molecules* **2020,** *25*.
31. Patel, D. S.; Qi, Y.; Im, W., Modeling and Simulation of Bacterial Outer Membranes and Interactions with Membrane Proteins. *Curr. Opin. Struc. Biol.* **2017,** *43*, 131-140.

32. Jorgensen, W. L.; Chandrasekhar, J.; Madura, J. D.; Impey, R. W.; Klein, M. L., Comparison of Simple Potential Functions for Simulating Liquid Water. *J. Chem. Phys.* **1983,** *79*, 926-935.
33. Neria, E.; Fischer, S.; Karplus, M., Simulation of Activation Free Energies in Molecular Systems. *J. Chem. Phys.* **1996,** *105*, 1902-1921.
34. Kim, S.; Patel, D. S.; Park, S.; Slusky, J.; Klauda, J. B.; Widmalm, G.; Im, W., Bilayer Properties of Lipid a from Various Gram-Negative Bacteria. *Biophys. J.* **2016,** *111*, 1750-1760.
35. Klauda, J. B.; Venable, R. M.; Freites, J. A.; O'Connor, J. W.; Tobias, D. J.; Mondragon-Ramirez, C.; Vorobyov, I.; MacKerell, A. D.; Pastor, R. W., Update of the Charmm All-Atom Additive Force Field for Lipids: Validation on Six Lipid Types. *J. Phys. Chem. B* **2010,** *114*, 7830-7843.
36. Guvench, O.; Greene, S. N.; Kamath, G.; Brady, J. W.; Venable, R. M.; Pastor, R. W.; Mackerell, A. D., Additive Empirical Force Field for Hexopyranose Monosaccharides. *J. Comput. Chem.* **2008,** *29*, 2543-2564.
37. Guvench, O.; Hatcher, E.; Venable, R. M.; Pastor, R. W.; MacKerell, A. D., Charmm Additive All-Atom Force Field for Glycosidic Linkages between Hexopyranoses. *J. Chem. Theory Comput.* **2009,** *5*, 2353-2370.
38. Hatcher, E.; Guvench, O.; MacKerell, A. D., Charmm Additive All-Atom Force Field for Aldopentofuranoses, Methyl-Aldopentofuranosides, and Fructofuranose. *J. Phys. Chem. B* **2009,** *113*, 12466-12476.
39. Guvench, O.; Mallajosyula, S. S.; Raman, E. P.; Hatcher, E.; Vanommeslaeghe, K.; Foster, T. J.; Jamison, F. W.; MacKerell, A. D., Charmm Additive All-Atom Force Field for Carbohydrate Derivatives and Its Utility in Polysaccharide and Carbohydrate-Protein Modeling. *J. Chem. Theory Comput.* **2011,** *7*, 3162-3180.
40. Park, S.-J.; Lee, J.; Patel, D. S.; Ma, H.; Lee, H. S.; Jo, S.; Im, W., Glycan Reader Is Improved to Recognize Most Sugar Types and Chemical Modifications in the Protein Data Bank. *Bioinformatics* **2017,** *33*, 3051-3057.
41. Ryckaert, J.-P.; Ciccotti, G.; Berendsen, H. J. C., Numerical Integration of the Cartesian Equations of Motion of a System with Constraints: Molecular Dynamics of N-Alkanes. *J. Comput. Phys.* **1977,** *23*, 327-341.
42. Steinbach, P. J.; Brooks, B. R., New Spherical-Cutoff Methods for Long-Range Forces in Macromolecular Simulation. *J. Comput. Chem.* **1994,** *15*, 667-683.
43. Essmann, U.; Perera, L.; Berkowitz, M. L.; Darden, T.; Lee, H.; Pedersen, L. G., A Smooth Particle Mesh Ewald Method. *J. Chem. Phys.* **1995,** *103*, 8577-8593.
44. Chow, K. H.; Ferguson, D. M., Isothermal Isobaric Molecular-Dynamics Simulations with Monte-Carlo Volume Sampling. *Comput. Phys. Commun.* **1995,** *91*, 283-289.
45. Aqvist, J.; Wennerstrom, P.; Nervall, M.; Bjelic, S.; Brandsdal, B. O., Molecular Dynamics Simulations of Water and Biomolecules with a Monte Carlo Constant Pressure Algorithm. *Chem. Phys. Lett.* **2004,** *384*, 288-294.
46. Klauda, J. B.; Eldho, N. V.; Gawrisch, K.; Brooks, B. R.; Pastor, R. W., Collective and Noncollective Models of Nmr Relaxation in Lipid Vesicles and Multilayers. *J. Phys. Chem. B* **2008,** *112*, 5924-5929.
47. Klauda, J. B.; Roberts, M. F.; Redfield, A. G.; Brooks, B. R.; Pastor, R. W., Rotation of Lipids in Membranes: Molecular Dynamics Simulation, 31P Spin-Lattice Relaxation, and Rigid-Body Dynamics. *Biophys. J.* **2008,** *94*, 3074-3083.

48. Monje-Galvan, V.; Klauda, J. B., Modeling Yeast Organelle Membranes and How Lipid Diversity Influences Bilayer Properties. *Biochemistry* **2015,** *54*, 6852-6861.

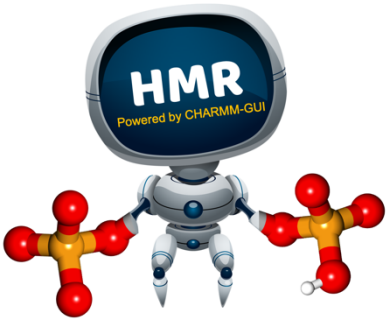

For Table of Contents Only